Bulletin of Mathematical Biology manuscript No.
(will be inserted by the editor)

Inside dynamics of integrodifference equations with mutations

Nathan G. Marculis · Mark A. Lewis

Received: date / Accepted: date

Abstract The method of inside dynamics provides a theory that can track the dynamics of neutral gene fractions in spreading populations. However, the role of mutations has so far been absent in the study of the gene flow of neutral fractions via inside dynamics. Using integrodifference equations, we develop a neutral genetic mutation model by extending a previously established scalar inside dynamics model. To classify the mutation dynamics, we define a mutation class as the set of neutral fractions that can mutate into one another. We show that the spread of neutral genetic fractions is dependent on the leading edge of population as well as the structure of the mutation matrix. Specifically, we show that the neutral fractions that contribute to the spread of the population must belong to the same mutation class as the neutral fraction found in the leading edge of the population. We prove that the asymptotic proportion of individuals at the leading edge of the population spread is given by the dominant right eigenvector of the associated mutation matrix, independent of growth and dispersal parameters. In addition, we provide numerical simulations to demonstrate our mathematical results, to extend their generality, and to develop new conjectures about our model.

Keywords integrodifference equations · mutations · neutral genetic diversity · range expansion · spreading speed

Acknowledgements This research was supported by a grant to MAL from the Natural Science and Engineering Research Council of Canada (grant no. NET GP 434810-12) to the TRIA Network, with contributions from Alberta Agriculture and Forestry, Foothills Research Institute, Manitoba Conservation and Water Stewardship, Natural Resources Canada-Canadian Forest Service, Northwest Territories Environment and Natural Resources, Ontario Ministry of Natural Resources and Forestry, Saskatchewan Ministry of Environment, West Fraser and Weyerhaeuser. MAL is also grateful for support through NSERC and the Canada Research

Nathan G. Marculis
Department of Mathematical and Statistical Sciences,
University of Alberta, Edmonton, AB T6G 2G1, Canada
E-mail: marculis@ualberta.ca

Mark A. Lewis
Department of Mathematical and Statistical Sciences & Department of Biological Sciences,
University of Alberta, Edmonton, AB T6G 2G1, Canada

Chair Program. NGM acknowledges support from NSERC TRIA-Net Collaborative Research Grant and would like to express his thanks to the Lewis Research Group for the many discussions and constructive feedback throughout this work. We are also grateful for the helpful and detailed comments from anonymous reviewers.

1 Introduction

The neutral theory of molecular evolution posits that most of the genetic variation in populations is independent of selection and hence is neutral (Duret, 2008). When this theory holds, it suggests that much of the variation in populations is due to events such as mutations or genetic drift, without the influence of selection. This provides support for including neutral mutation dynamics into models of genetic spread. The molecular clock hypothesis states that genes evolve at a relatively constant rate over time (Bromham and Penny, 2003). We use this hypothesis in our model formulation by assuming the rate of mutation of one gene to another is constant over time. This theory suggests the genetic difference between any two species is proportional to the time since these species last shared a common ancestor. Therefore, if the molecular clock hypothesis is true, this can be used for estimating evolutionary timescales (Ho, 2008).

Neutral genetic patterns caused by range expansions is a topic of recent scientific and modeling interest (Hallatschek and Nelson, 2008). The establishment of a new population undertaken by a few original founders who carry only a small fraction of the total genetic variation of the parental population is referred to as the founder effect (Mayr, 1940). Range expansions are commonly thought to reduce the genetic diversity of a population due to the founder effect. When a population is expanding its range, consecutive founder events result in the phenomena known as gene surfing (Excoffier and Ray, 2008). This is the spatial analog of genetic drift and occurs when certain alleles reach higher than expected frequencies at the front of a range expansion (Slatkin and Excoffier, 2012). However in the presence of neutral mutations, these processes may be altered. We are not the first to model this problem; previous studies have used simulation based models (Edmonds et al., 2004; Klopfstein et al., 2006) and lab experiments (Hallatschek et al., 2007) to understand the effects of neutral mutations on the wave of range expansions. On a related front, others have also developed theoretical models to understand metapopulation dynamics of gene flow from one population to another (Lande, 1992; Lynch, 1988; Pannell and Charlesworth, 1999, 2000; Slatkin, 1985). However, none have incorporated mutations between neutral genetic fractions into an analytical population spread model such as a reaction-diffusion, integrodifference, or integrodifferential equations.

Integrodifference equations have played a central role in studying problems in theoretical ecology such as range expansions (Krkošek et al., 2007; Zhou and Kot, 2011), the spread of invasive species (Bateman et al., 2017; Kot et al., 1996; Lewis et al., 2016), determining the critical domain size for population persistence (Lutscher et al., 2005; Reimer et al., 2016; Van Kirk and Lewis, 1997), and more recently understanding the neutral genetic structure of populations (Lewis et al., 2018; Marculis et al., 2017, 2019). In this work, we aim to understand role that mutations play in the neutral genetic diversity of a population undergoing range expansion by studying the process via an integrodifference equation model.

Yhe classical integrodifference equation is

$$u_{t+1}(x) = \int_{-\infty}^{\infty} k(x-y)g(u_t(y))u_t(y)\,dy \tag{1}$$

where u_t is the population density at time t, k is the dispersal kernel describing dispersal from y to x, g is the per-capita growth function, and $u_0(x)$ is the initial population distribution in space. To understand the role that mutations play on the neutral genetic diversity of a spreading population, we study the inside dynamics of integrodifference equations with neutral mutations. The term *inside dynamics* refers to changes in the inside structure of the population rather than in the total density. The key assumption in the analysis of inside dynamics is that all individuals grow and disperse in the same manner, differing only with respect to neutral genetic markers. In other words, all individuals in the population have the same fitness. This allows us to partition the population into distinct subgroups called neutral fractions and track the spatio-temporal evolution of these subgroups. By making the assumption of neutral fractions with no mutations, we obtain the following system of equations for the inside dynamics of our scalar integrodifference equation,

$$v^i_{t+1}(x) = \int_{-\infty}^{\infty} k(x-y)g(u_t(y))v^i_t(y)\,dy, \text{ for } i = 1,\dots,n, \tag{2}$$

where n is the finite number of neutral fractions and $u_t(x) = \sum_{i=1}^{n} v^i_t(x)$.

Inside dynamics have been studied for a variety of different spatio-temporal population models, including reaction-diffusion equations (Garnier and Lewis, 2016; Garnier et al., 2012; Roques et al., 2012, 2015), delay reaction-diffusion equations (Bonnefon et al., 2013), integro-differential equations (Bonnefon et al., 2014), and integrodifference equations (Lewis et al., 2018; Marculis et al., 2017, 2019). The three previous studies on integrodifference equations analyzed a scalar model (Marculis et al., 2017), a model with climate change (Lewis et al., 2018), and a stage-structured population model (Marculis et al., 2019). Our extension to these previous works is to analyze the inside dynamics of a scalar integrodifference equation with mutations between neutral fractions. By comparing the differences between our model and those previously studied, we gain insight regarding the role of mutations in the spread of neutral genetic markers.

Mutations between neutral fractions are called neutral mutations because there is no direct effect on the fitness of the individual. This process adds a level of biological complexity and including it into a model increases the biological realism. The addition of neutral mutations to the model is important for realism because it is a natural process that is known to occur and can be used in studying molecular clocks to identify evolutionary events such as speciation and evolutionary radiation. For our analyses, we are interested in how the addition of neutral mutations into the modeling structure can impact the resulting patterns of genetic spread.

The organization of the paper is as follows: Section 2 provides a derivation of our mutation matrix model. That is, we extend (2) to include mutations between neutral fractions. In Section 3, we lay out some preliminary material and assumptions that will be used in the main theorems. Once the preliminary material has been established, we move on to the main results. Here, we state four main theorems about the asymptotic spread of the neutral fractions in Section 4.

In Section 5, we perform some numerical simulations to support our main results and understand how different components affect the asymptotic dynamics. These simulations lead to conjectures regarding which assumptions in the main theorems could be relaxed without changing the results. Finally, in Section 6, we provide a discussion of the work including model development, outcomes, limitations, and future directions.

2 Mutation matrix model

Our goal is to extend the system of equations (2) to include neutral mutations that happen during reproduction. To do this, we must determine how to incorporate mutations into the model. A common method, which has been previously used to study the mutations of DNA, is to use the substitution model. A substitution model describes the process of genetic variation by which one variant is replaced with another, at a given constant mutation rate (Arenas, 2015). To model the substitution process, continuous-time Markov chains are a common tool of choice. The first and simplest substitution model was developed by Jukes and Cantor for the mutation of DNA base pairs in amino acids (Jukes and Cantor, 1969) . This model assumes equal base frequencies and equal mutation rates, giving a simplistic one parameter depiction. Others have added complexity to the Jukes Cantor model by distinguishing between types of transitions (Kimura, 1980), and by allowing the base frequencies to vary (Felsenstein, 1981). In all of these models, the dynamics are driven by the rate matrix for the continuous-time Markov chain.

In our work, we are not concerned with modeling DNA sequence evolution in amino acids, but, rather, the change of neutral genetic markers in an organism which reproduces at discrete time intervals. To achieve this, we use a modeling framework similar to substitution models, but via a discrete-time Markov chain. Since our neutral fraction model is an integrodifference equation and we are assuming that the mutations are occurring during reproduction, a discrete-time Markov chain is suitable to model the mutation process. Thus, we can construct a mutation matrix with entries describing the mutation probabilities. Consider a single locus with n different neutral alleles and let $0 < m_{jl} < 1$ be the probability of mutation from a type l to a type j individual and $\mathbf{v} = \left[v^1, v^2, \ldots, v^n\right]^T$. Then, we obtain the following equation

$$\mathbf{v}_{t+1}(x) = \int_{-\infty}^{\infty} k(x-y)\mathbf{M}g(u_t(y))\mathbf{v}_t(y)\,dy, \tag{3}$$

where $u_t(x) = \sum_{i=1}^{n} v_t^i(x)$, $\mathbf{M}$ is the mutation matrix given by

$$\mathbf{M} = \begin{bmatrix} 1-\sum_{j\neq 1} m_{j1} & m_{12} & \ldots & m_{1(n-1)} & m_{1n} \\ m_{21} & 1-\sum_{j\neq 2} m_{j2} & \ldots & m_{2(n-1)} & m_{2n} \\ \vdots & \vdots & \ddots & \vdots & \vdots \\ m_{(n-1)1} & m_{(n-1)2} & \ldots & 1-\sum_{j\neq n-1} m_{j(n-1)} & m_{(n-1)n} \\ m_{n1} & m_{n2} & \ldots & m_{n(n-1)} & 1-\sum_{j\neq n} m_{jn} \end{bmatrix}, \tag{4}$$

and our initial condition, $\mathbf{v}_0(x)$, satisfies

$$\sum_{i=1}^{n} v_0^i(x) = u_0(x). \tag{5}$$

It should be noted that the same general form of the mutation matrix (4) can be attained by assuming there are m loci with a different neutral alleles where $n = a^m$; see Appendix A. Thus, our model is quite general and could be applied to commonly studied neutral genetic marks such as microsatellite data (Selkoe and Toonen, 2006) or mutations by single nucleotide polymorphisms (SNPs) (Morin et al., 2004). In particular, to study the effects of SNPs on a single locus the mutation matrix will have dimensions 4×4 to account for the mutation rates between the four nucleotides. Our mutation matrix model given in (3) is different from the scalar model in (2) because there are interactions between the neutral fractions. Thus, for our analysis we must consider all neutral fractions rather than focusing on a single neutral fraction as done in previous studies for the scalar model.

Definition 1 A square matrix is called a *Markov matrix* if all entries are nonnegative and the sum of each column vector is equal to one.

Note that the mutation matrix given in (4) is Markov. One consequence of a Markov matrix, which we will frequently use throughout our work, is that the dominant eigenvalue is equal to one. The mutation matrix given in (4) is a Markov matrix. If $\mathbf{M}$ is irreducible then it is possible to mutate from any given genotype to any other genotype in a finite number of steps. A stricter version of irreducibility is primitivity. If $\mathbf{M}$ is primitive then there exists a t such that it is possible to mutate from any given neutral genotype to any other in exactly t steps (i.e. $\mathbf{M}^t > \mathbf{0}$). We assume that this is the case. Recall that a nonnegative matrix is primitive if it is irreducible and all the entries on the diagonal are strictly positive. Thus, by assuming primitivity instead of irreducibility for the mutation matrix means that at each time step for each neutral fraction there are some individuals that do not mutate into another type. In our work we consider Markov matrices that are not necessarily primitive but are block diagonal primitive.

Definition 2 A square matrix $\mathbf{M}$ is *block diagonal primitive* if for some $t > 0$, $\mathbf{M}^t$ can be written as a block diagonal matrix where each block is primitive. That is, we can express

$$\mathbf{M}^t = \begin{bmatrix} \mathbf{M}_1^t & 0 & \dots & 0 \\ 0 & \mathbf{M}_2^t & \dots & 0 \\ \vdots & \vdots & \ddots & \vdots \\ 0 & 0 & \dots & \mathbf{M}_b^t \end{bmatrix} \tag{6}$$

where $\mathbf{M}_q^t > 0$ for $q = 1, \dots, b$.

In what follows, we make the following assumption:

$A1:$ *The matrix* $\mathbf{M}$ *is Markov and block diagonal primitive.*

.

A consequence of the mutation matrix being a nontrivial block diagonal primitive matrix is that neutral fractions can only mutate into a select subset of the different types. The block primitive assumption is much more general than primitivity and allows us to study models where the mutations of alleles occurs for b different mutation classes. We next define a set that encompasses how the neutral fractions can mutate.

Definition 3 Neutral fraction i is in the mutation class q if $m_{il} \in \mathbf{M}_q$ for some l.

To connect the concepts of Definitions 2 and 3 we consider a graphical representation of the mutation matrix. In particular, from Definition 2, we can see that the mutation matrix $\mathbf{M}$ is actually comprised of b disjoint sub-matrices which describe b different mutation classes. Thus, if we were to represent the mutation matrix as a graph, we would have b disconnected graphs where the nodes correspond to the n neutral fractions and each sub-graph is connected by the entries from the mutation matrix. Thus, it is natural to interpret the b disconnected subgraphs are the mutation classes outlined in Definition 3. For example, a mutation matrix with two mutation classes $\{1,2\}$ and $\{3,4,5\}$ would have two blocks $\mathbf{M}_1$ and $\mathbf{M}_2$ and be given by

$$\mathbf{M} = \begin{bmatrix} \mathbf{M}_1 & \mathbf{0} \\ \mathbf{0} & \mathbf{M}_2 \end{bmatrix} \tag{7}$$

$$= \begin{bmatrix} 1-m_{21} & m_{12} & 0 & 0 & 0 \\ m_{21} & 1-m_{12} & 0 & 0 & 0 \\ 0 & 0 & 1-m_{43}-m_{53} & m_{34} & m_{35} \\ 0 & 0 & m_{43} & 1-m_{34}-m_{54} & m_{45} \\ 0 & 0 & m_{53} & m_{54} & 1-m_{35}-m_{45} \end{bmatrix}. \tag{8}$$

We provide a graphical interpretation of this mutation matrix in Figure 1. Note that by our assumption that the mutation matrix is block diagonal makes it is clear that the mutation classes are independent and disconnected from one another. Thus, without loss of generality in our analysis, we are able to focus on mutations within a single class.

3 Spreading properties of integrodifference equations

In this work, we consider spreading populations that take the form of traveling waves. That is, $u_t(x) = U(x - ct)$ where c is the wave speed. In the analysis that follows, we frequently use the classical result for the spreading speed of a population introduced over a compact region. That is, when the maximum per-capita growth is at the lowest densities,

$A2:\ 0 < g(u) \leq g(0)$ *for all* $u \in (0,1)$,

k is thin-tailed (i.e., has a moment generating function), and the operator is order preserving, we can compute the rightward spreading speed for (1) with the following formula,

$$c^* = \inf_{s>0} \frac{1}{s} \ln\left(g(0) \int_{-\infty}^{\infty} k(x) e^{sx}\, dx \right) \tag{9}$$

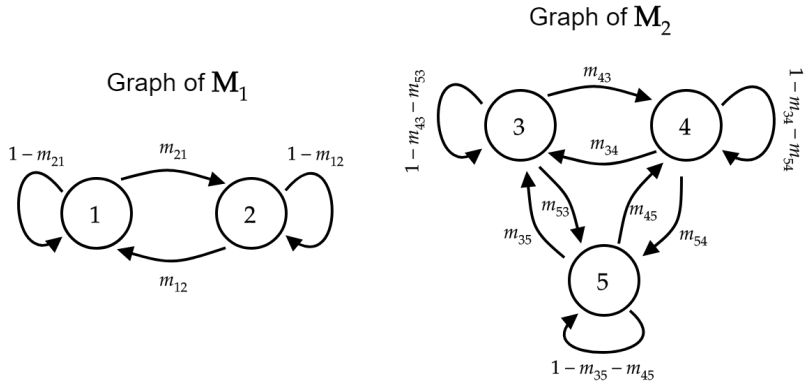

Fig. 1 Here we provide a graphical representation of the sample mutation matrix provided in (8).

(Weinberger, 1982). In this formula we interpret s as the exponential decay profile at the leading edge of the traveling wave solution. We also know from Weinberger (1982) that there exists a family of traveling wave solutions parameterized by speed c for $c \geq c^*$. We can find the leftward spreading speed with a calculation similar to (9),

$$c_-^* = \inf_{s>0} \frac{1}{s} \ln \left(g(0) \int_{-\infty}^{\infty} k(x) e^{-sx}\, dx \right). \tag{10}$$

In particular, when we assume that

*A*3 : *k is Gaussian with mean* μ *and variance* σ^2*,*

the kernel is given by

$$k(x;\mu,\sigma) = \frac{1}{\sqrt{2\pi\sigma^2}} e^{-\frac{(x-\mu)^2}{2\sigma^2}}. \tag{11}$$

Then, we can calculate the rightward spreading speed to be

$$c^* = \sqrt{2\sigma^2 \ln(g(0))} + \mu, \tag{12}$$

and in a similar fashion the leftward spreading speed is

$$c_-^* = \sqrt{2\sigma^2 \ln(g(0))} - \mu. \tag{13}$$

A fourth assumption that will be made in our theorems in the next section is related to the decay rate of the initial condition. If we consider a traveling wave that spreads with speed $c \geq c^*$, then the decay properties for the leading edge of the wave can be derived from Proposition 3 in Lui (1983). To compute the critical decay rate for the rightward spread we solve for the unique value of s that satisfies (9) for the rightward spread. In the case when the dispersal kernel is Gaussian, we can explicitly solve for this value of s and obtain the value $\frac{c-\mu}{\sigma^2}$. Similarly, for the leftward spread, the critical decay rate for the leftward spread is the unique value of s that satisfies (10). In the case when the dispersal kernel is Gaussian, we can explicitly solve for this value of s and obtain the value $\frac{c+\mu}{\sigma^2}$. When $c > c^*$,

then the decay of the rightward traveling wave is $A_c e^{-\frac{c-\mu}{\sigma^2}x}$ at ∞ and the decay of the leftward traveling wave is $A_c e^{\frac{c+\mu}{\sigma^2}x}$ at $-\infty$ where A_c is a positive constant. When $c = c^*$, then the decay of the rightward traveling wave is $A_{c^*} x e^{-\frac{c-\mu}{\sigma^2}x}$ at ∞ and the decay of the leftward traveling wave is $A_{c^*} x e^{\frac{c+\mu}{\sigma^2}x}$ at $-\infty$ where A_{c^*} is a positive constant. In each of the four theorems, which we present in the next section, the precise form of the fourth assumption differs. Thus, we do not explicitly write out the different assumptions here, but save them for the statement of the theorems. With the definitions, assumptions, and preliminary material in place, we can present the main results of the paper.

4 Asymptotic results

In this section, we provide some theoretical results for the asymptotic dynamics of our model given by (3)-(5). Here, we state the four main theorems about the asymptotic spread of the neutral fractions. To recap, we make the following assumptions on Equation (3):

$A1:$ *The matrix* $\mathbf{M}$ *is Markov and block diagonal primitive,*
$A2:$ $0 < g(u) \leq g(0)$ *for all* $u \in (0,1)$*, and*
$A3:$ k *is Gaussian with mean* μ *and variance* σ^2*.*

Assumption $A1$ (Markov and block diagonal primitive matrix) is needed so we can apply the Perron-Frobenius theorem to each block in our analysis. Assumption $A2$ (maximum per-capita growth rate as density approaches zero) is relevant to expanding populations exhibiting "pulled" wave dynamics (Stokes, 1976), where the leading edge of the wave determines the spreading speed (9). Assumption $A3$ (a Gaussian dispersal kernel) is made for mathematical convenience. This will allow us to prove rigorous results about the resulting system.

Theorem 1 provides sufficient conditions for when neutral fractions in a given mutation class are left behind during the population spread and do not contribute to the spread of the population. In other words, Theorem 1 states that if there are no neutral fractions in a given mutation class at the leading edge, then all members of this mutation class converge to zero uniformly in the moving half-frame.

Theorem 1 *Consider* (3)-(5) *where* $A1$-$A3$ *hold as well as the additional assumption:*

$A4:$ $\int_{-\infty}^{\infty} e^{\frac{c-\mu}{\sigma^2}y} v_0^i(y)\, dy < \infty$ *for every* i *in mutation class* q*.*

If $c \geq c^*$*, then for any* $A \in \mathbb{R}$*, the density of the neutral fraction* i*,* $v_t^i(x)$*, converges to* 0 *uniformly as* $t \to \infty$ *in the moving half-frame* $[A + ct, \infty)$*.*

Theorem 1 gives conditions for when neutral fractions for a rightward spreading population to converge to zero in the moving half-frame. We can also consider the case when we have a leftward spreading population in the following theorem.

Theorem 2 *Consider* (3)-(5) *where* $A1$-$A3$ *hold as well as the additional assumption:*

$A4^-:$ $\int_{-\infty}^{\infty} e^{-\frac{c+\mu}{\sigma^2}y} v_0^i(y)\, dy < \infty$ *for every* i *in mutation class* q*.*

If $c \geq c_-^*$, then for any $A \in \mathbb{R}$, the density of the neutral fraction i, $v_t^i(x)$, converges to 0 uniformly as $t \to \infty$ in the moving half-frame $(-\infty, A - ct]$.

From Theorems 1 and 2 we conclude that if each neutral fraction in a given mutation class is not located at the leading edge of the traveling wave in the sense of $A4$ or $A4^-$ respectively, then these neutral fractions will converge to zero in the moving half-frame. Thus, these neutral fractions are not able to keep up with the traveling wave which shows erosion of diversity inside such fronts. The question remains as to what happens to the neutral fractions at the leading edge and to the rest of the neutral fractions in the same mutation class. The next two theorems provide asymptotic results for these neutral fractions for a particular class of initial data where neutral fractions are proportional to the exponentially decaying leading edge of the wave.

Theorem 3 *Consider* (3)-(5) *where* $A1$-$A3$ *hold as well as the additional assumption:*

$A4'$: *Individuals in mutation class q are initially present at the leading edge of the front in the sense that*

$$\frac{\mathbf{v}_0(x)^T \boldsymbol{\ell}_q / \left(\mathbf{r}_q^T \boldsymbol{\ell}_q\right)}{u_0(x)} \to p_0^q > 0 \text{ as } x \to \infty \tag{14}$$

and

$$\int_{-\infty}^{\infty} e^{\frac{c-\mu}{\sigma^2} y} \left| \frac{\mathbf{v}_0(y)^T \boldsymbol{\ell}_q}{\mathbf{r}_q^T \boldsymbol{\ell}_q} - p_0^q u_0(y) \right| dy < \infty \tag{15}$$

where $\mathbf{r}_q$ the eigenvector of $\mathbf{M}$ associated to the eigenvalue 1 from the matrix $\mathbf{M}_q$ and $\boldsymbol{\ell}_q$ be the eigenvector of $\mathbf{M}^T$ associated to the eigenvalue 1 from the matrix $\mathbf{M}_q^T$.

Then, for $c \geq c^*$ and any $A \in \mathbb{R}$,

$$\max_{[A+ct,\infty)} \left\| \mathbf{v}_t(x) - \sum_{q=1}^{n_q} p_0^q u_t(x) \mathbf{r}_q \right\| \to 0 \text{ as } t \to \infty. \tag{16}$$

Theorem 3 provides the asymptotic proportion of each neutral fraction in mutation class q for the rightward spread. In particular, if individuals from only one mutation class q are intially present at the leading edge of the population then this proportion is simply $\mathbf{r}_q$, the right eigenvector of $\mathbf{M}_q$ corresponding to eigenvalue 1. We can also compute the leftward proportion in the following theorem.

Theorem 4 *Consider* (3)-(5) *where* $A1$-$A3$ *hold as well as the additional assumption:*

$A4'^-$: *Individuals in mutation class q are initially present at the leading edge of the front in the sense that*

$$\frac{\mathbf{v}_0(x)^T \boldsymbol{\ell}_q / \left(\mathbf{r}_q^T \boldsymbol{\ell}_q\right)}{u_0(x)} \to p_0^q > 0 \text{ as } x \to -\infty \tag{17}$$

and

$$\int_{-\infty}^{\infty} e^{-\frac{c+\mu}{\sigma^2}y} \left| \frac{\mathbf{v}_0(y)^T \boldsymbol{\ell}_q}{\mathbf{r}_q^T \boldsymbol{\ell}_q} - p_0^q u_0(y) \right| dy < \infty \tag{18}$$

where $\mathbf{r}_q$ *the eigenvector of* $\mathbf{M}$ *associated to the eigenvalue* 1 *from the matrix* $\mathbf{M}_q$ *and* $\boldsymbol{\ell}_q$ *be the eigenvector of* $\mathbf{M}^T$ *associated to the eigenvalue* 1 *from the matrix* $\mathbf{M}_q^T$.

Then, for $c \geq c_-^*$ *and any* $A \in \mathbb{R}$,

$$\max_{(-\infty, A-ct]} \left\| \mathbf{v}_t(x) - \sum_{q=1}^{n_q} p_0^q u_t(x) \mathbf{r}_q \right\| \to 0 \text{ as } t \to \infty. \tag{19}$$

The proofs of Theorems 1-4 are provided in Appendix B.

5 Numerical simulations

In this section we illustrate our theory in Section 4 with some simple examples. All simulations were done by using the fast Fourier transform technique (Cooley and Tukey, 1965). This method is better than classical quadrature because it speeds up the numerical process from $O(n^2)$ to $O(n \log(n))$.

For our first set of simulations, we consider an example where the Assumptions $A1$, $A2$, and $A3$ are satisfied. Specifically, we assume that k is a Gaussian dispersal kernel and g is the Beverton-Holt growth function. That is, k is given by (11) and

$$g(u_t(y)) = \frac{R}{1 + \frac{R-1}{K} u_t(y)}. \tag{20}$$

The model we simulate is

$$\mathbf{v}_{t+1}(x) = \int_{-\infty}^{\infty} \frac{1}{\sqrt{2\pi\sigma^2}} e^{-\frac{(x-y-\mu)^2}{2\sigma^2}} \frac{R}{1 + \frac{R-1}{K} u_t(y)} \mathbf{M}\mathbf{v}_t(y)\, dy \tag{21}$$

where $\mathbf{M}$ is the mutation matrix. In this section, we consider a few different mutation matrices. The first mutation matrix is primitive and allows for mutations between all neutral fractions. This matrix is given by

$$\mathbf{M1} = \begin{bmatrix} 0.85 & 0.01 & 0.04 & 0.02 & 0.03 \\ 0.03 & 0.92 & 0.02 & 0.01 & 0.05 \\ 0.07 & 0.05 & 0.86 & 0.02 & 0.03 \\ 0.01 & 0.01 & 0.06 & 0.93 & 0.03 \\ 0.04 & 0.01 & 0.02 & 0.02 & 0.86 \end{bmatrix}. \tag{22}$$

The second mutation matrix we consider is block primitive. Here, the parameters are the same as in **M1** except we let $m_{13} = m_{14} = m_{15} = m_{23} = m_{24} = m_{25} = m_{31} = m_{32} = m_{41} = m_{42} = m_{51} = m_{52} = 0$. Then **M2** is given by

$$\mathbf{M2} = \begin{bmatrix} 0.97 & 0.01 & 0 & 0 & 0 \\ 0.03 & 0.99 & 0 & 0 & 0 \\ 0 & 0 & 0.92 & 0.02 & 0.03 \\ 0 & 0 & 0.06 & 0.96 & 0.03 \\ 0 & 0 & 0.02 & 0.02 & 0.94 \end{bmatrix}. \tag{23}$$

Notice that **M2** is block primitive because it only allows for mutations between two distinct classes of neutral fractions. The two mutation classes are given by $\{1, 2\}$ and $\{3, 4, 5\}$. Thus, neutral fractions 1 and 2 can mutate into each other but not into neutral fractions 3, 4, and 5 and vice-versa.

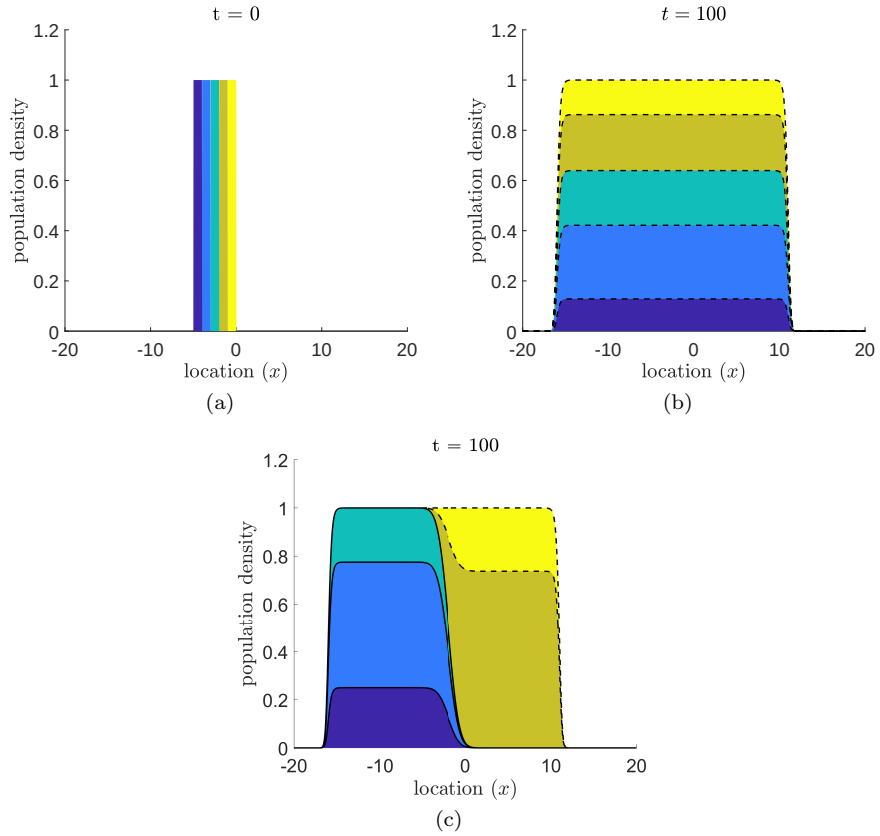

Fig. 2 Numerical realization of (21) for the parameter values $\sigma^2 = 0.01$, $\mu = 0$, $R = 2$, $K = 1$. Figure 2(a) is the initial condition for the simulations seen in Figures 2(b) and 2(c). In 2(b) we use the mutation matrix **M1** given by (22). The dashed lines in Figure 2(b) give the asymptotic proportion of neutral fractions as calculated in Theorem 3. In 2(c) we use the mutation matrix **M2** given by (23). The dashed lines in Figure 2(c) give the rightward asymptotic proportion of neutral fractions as calculated in Theorem 3 and the solid lines in Figure 2(c) give the leftward asymptotic proportion of neutral fractions as calculated in Theorem 4.

The simulations for our model are given in Figure 2. We chose these initial conditions so as to satisfy Assumptions $A4$ (see Theorem 1) and $A4^-$ (see Theorem 2). However, note that the initial conditions plotted in Figure 2(a) are not the same as those assumed by $A4'$ and $A4'^-$ for Theorems 3 and 4. These initial data were chosen in an effort to see if the results of the theorems could hold for a more general class of initial data than was assumed in the statement of the theorems. The initial density of each neutral fraction is given by $v_0^i(x) = \mathbb{1}_{-i<x\leq-(i-1)}$ where

$\mathbb{1}$ is the indicator function. In Figure 2(b), we are using the mutation matrix **M1** given by (22) where there is only one mutation class. Thus, the stable distribution of neutral fraction is calculated using Theorems 3 and 4 and is given by $\mathbf{r}_1 = [0.1377, 0.2229, 0.2179, 0.2932, 0.1283]^T$. The stable distribution can be seen by the dashed lines in Figure 2(b). In Figure 2(c), we use the mutation matrix **M2** given by (23) and we can see that the spread to the right and left have different neutral fractions because of the initial distribution of neutral fractions and because the structure of the mutation matrix is block diagonal primitive with two blocks. The asymptotic distribution of neutral fractions for the first mutation class $\{1, 2\}$ in the rightward spread is calculated by Theorem 3 and is given by $\mathbf{r}_1 = [0.25, 0.75]^T$. This is seen by the dashed lines in Figure 2(c). The asymptotic distribution of neutral fractions for the second mutation class $\{3, 4, 5\}$ in the leftward spread is calculated by Theorem 4 and is given by $\mathbf{r}_2 = [0.225, 0.525, 0.25]^T$. This is seen by the solid lines in Figure 2(c).

In this section, we also would like to understand dynamics of mutation matrices that do not satisfy Assumptions $A1$ and $A3$ of Theorems 1-4. In particular, we want to consider matrix structures that do not fit to the block diagonal primitive assumption, and dispersal kernels that are not Gaussian. We first, consider the Laplace dispersal kernel,

$$k(x-y) = \frac{1}{2b} e^{-|x-\mu|/b} \tag{24}$$

again with Beverton-Holt growth given by (20). Then the model that we simulate is given by

$$\mathbf{v}_{t+1}(x) = \int_{-\infty}^{\infty} \frac{1}{2b} e^{-|x-\mu|/b} \frac{R}{1 + \frac{R-1}{K} u_t(y)} \mathbf{M}\mathbf{v}_t(y)\, dy. \tag{25}$$

For our simulations, we want to compare the effect of the dispersal kernel on the asymptotic proportion of neutral fractions. Thus, we run simulations similar to those in Figure 2 by using the same demographic parameters and mutation matrices, but we use a Laplace dispersal kernel.

The simulations for our model are given in Figure 3. The initial conditions are plotted in Figure 3(a) and are the same initial conditions used for the simulations in Figure 2. The initial density of each neutral fraction is given by $v_0^i(x) = \mathbb{1}_{-i<x\leq-(i-1)}$ where $\mathbb{1}$ is the indicator function. In Figure 3(b) since we are using the mutation matrix **M1** given by (22) there is only one mutation class. We can see that the stable distribution of neutral fraction is given by $\mathbf{r}_1 = [0.1377, 0.2229, 0.2179, 0.2932, 0.1283]^T$ and is the same distribution as calculated using Theorems 3 and 4. This suggests that the dispersal kernel does not affect the asymptotic proportion, as expected, since the asymptotic proportion calculated by our main theorems is independent of the dispersal parameters. The stable distribution can be seen by the dashed lines in Figure 3(b). In Figure 3(c), we can see that the spread to the right and left have different neutral fractions because of the initial distribution of neutral fractions and because the mutation matrix **M2** given by (23) is block diagonal primitive with two blocks. The asymptotic distribution of neutral fractions for the first mutation class $\{1, 2\}$ in the rightward spread is $\mathbf{r}_1 = [0.25, 0.75]^T$. This is seen by the dashed lines in Figure 3(c). The asymptotic distribution of neutral fractions for the second mutation class $\{3, 4, 5\}$ in the leftward spread is $\mathbf{r}_2 = [0.225, 0.525, 0.25]^T$. This is seen

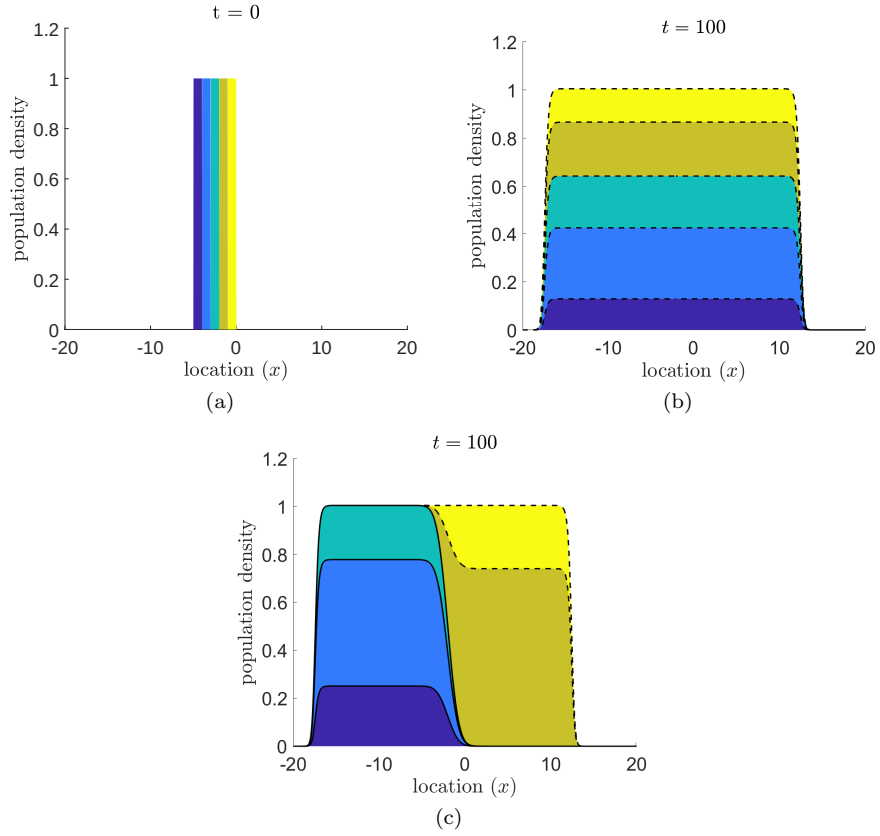

Fig. 3 Numerical realization of (25) for the parameter values $b = \sqrt{0.005}$, $\mu = 0$, $R = 2$, $K = 1$. We chose b and μ this way so that the mean and variance for the Laplace kernel is the same as the Gaussian kernel used for the simulations in Figure 2. Figure 3(a) is the initial condition for the simulations seen in Figures 3(b) and 3(c). In 3(b) we use the mutation matrix **M1** given by (22). The dashed lines in Figure 3(b) give the asymptotic proportion of neutral fractions as calculated in Theorem 3. In 3(c) we use the mutation matrix **M2** given by (23). The dashed lines in Figure 3(c) give the rightward asymptotic proportion of neutral fractions and the solid lines in Figure 3(c) give the leftward asymptotic proportion of neutral fractions.

by the solid lines in Figure 3(c). Notice that these proportions are again the same as suggested by Theorems 3 and 4.

Next, we consider a mutation matrix where the mutation classes are weakly linked. An example of this can be seen in the following matrix,

$$\mathbf{M3} = \begin{bmatrix} 0.97 & 0.01 & 0 & 0 & 0 \\ 0.03 & 0.99 & \varepsilon & 0 & 0 \\ 0 & 0 & 0.92-\varepsilon & 0.02 & 0.03 \\ 0 & 0 & 0.06 & 0.96 & 0.03 \\ 0 & 0 & 0.02 & 0.02 & 0.94 \end{bmatrix} \tag{26}$$

where ε is small. In this scenario, we see that there is only one mutation class because of the weak linkage parameter ε. This matrix structure violates Assump-

tion $A3$ because it is not block primitive as the bottom left block of the matrix is always zero. The structure of this matrix suggests that eventually all neutral fractions should become one of the first two types. For our simulation with this mutation matrix, we use a Gaussian dispersal kernel and Beverton-Holt growth function as given by (21). We can see a simulation of this in Figure 4.

For the mutation matrix **M3** we can see that it has one eigenvalue of 1 with eigenvector $\mathbf{r}_1 = [0.25, 0.75, 0, 0, 0]$. Thus, in this scenario, we conjecture that the asymptotic distribution of neutral fractions is given by $\mathbf{r}_1$. To test this conjecture, we simulate the model in Figure 4. One thing to note from Figure 4 is the amount time it takes to converge to the asymptotic proportion. Here we see that the leftward moving front takes over two thousand generations to reach the steady state. This is due to the fact that there is only one weak linkage, ε, from $\{3, 4, 5\}$ to $\{1, 2\}$. Note that this kind of behavior can also occur for a matrix that is irreducible but not primitive because the eigenvector has entries that are zero.

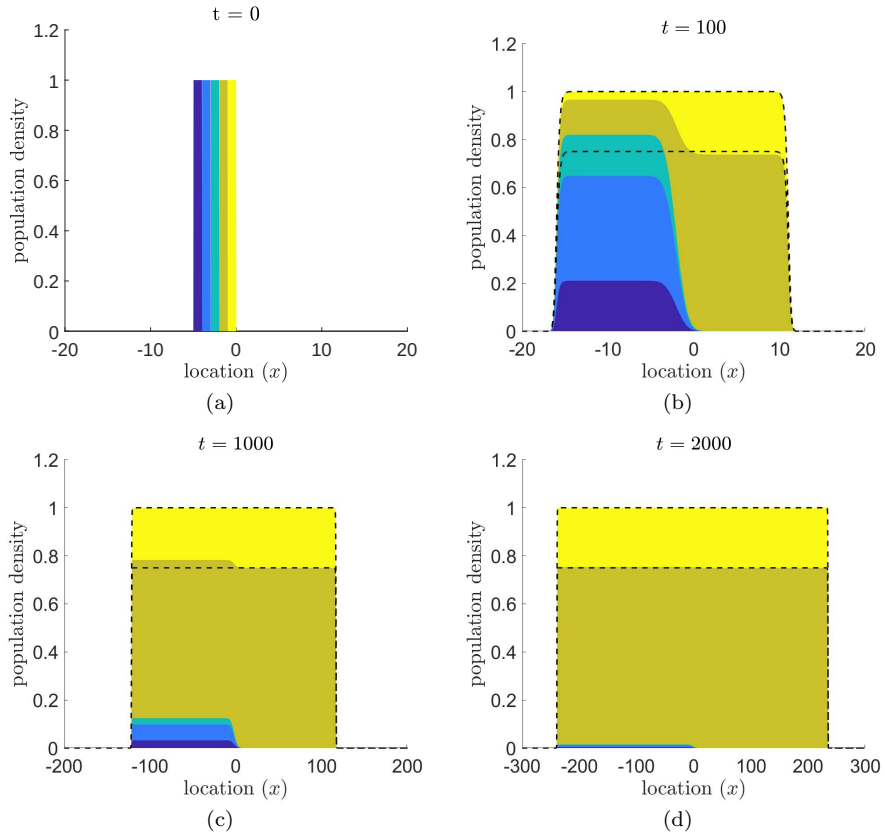

Fig. 4 Numerical realization of (21) for the parameter values $\sigma^2 = 0.01$, $\mu = 0$, $R = 2$, $K = 1$ with the mutation matrix **M3** given by (26) where $\varepsilon = 0.01$. Figure 2(a) is the initial condition for the simulations seen in Figures 4(b), 4(c), and 4(d). The dashed lines in Figure 4(b), 4(c), and 4(d) are the conjectured asymptotic proportion of neutral fractions.

6 Discussion

By incorporating mutations of neutral fractions into a scalar inside dynamics model, we developed a neutral mutation model to study the effect of mutations on the neutral genetic structure of an expanding population. In previous studies concerning the inside dynamics for scalar population models, the analysis concerns a single neutral fraction at a time (Marculis et al., 2017). In our model, the interactions between the neutral fractions by mutation require us to analyze a system of equations for the neutral fractions. By studying a system we must include an assumption on the interactions so as to prove the asymptotic results presented in Section 4.

We derive our model from the scalar inside dynamics integrodifference equation in Section 2. To include the mutations in our model, we allow for neutral fractions to mutate into one another with a given probability. The molecular clock hypothesis states that genes evolve at a relatively constant rate over time (Ho, 2008). Thus, our model is in line with the molecular clock hypothesis because we assume a constant probability of mutation over time. This modeling framework is commonly referred to in the genetic literature as a substitution model. The addition of mutations changes the model by now having interactions between neutral fractions that are governed by a mutation matrix.

The results in Section 4 are divided into four theorems. We first show when neutral fractions converge to zero uniformly in a moving half-frame. These results are provided in Theorems 1 and 2. We see that this happens when the neutral fractions in a given mutation class are not initially present at the leading edge of the expansion. In Theorems 3 and 4, we show that the only neutral fractions that matter are those at the leading edge and are in the accompanying mutation class. Moreover, Theorems 3 and 4 show that the proportion of neutral fractions is given by the right dominant eigenvector of the mutation matrix for the mutation class that was initially present at the leading edge of the population.

Our results only apply to a certain class of models. First, we make the assumption that the mutation matrix is block diagonal primitive on top of the Markov structure. This assumption is needed to apply the Perron-Frobenius theorem guaranteeing that we have a dominant eigenvalue. In Figure 2, we consider two different kinds of mutation matrices. The first mutation matrix is primitive and only contains one mutation class because every neutral fraction can mutate into one another. Thus, we see that all neutral fractions contribute the spread of the population and each neutral fraction converges to a proportion of the traveling wave solution. The result of the simulation is seen in Figure 2(b). In the second example, the mutation matrix has two mutation classes and we see the spread of one mutation class to the right and the spread of the other mutation class to the left in Figure 2(c). This is because of the initial positioning of the neutral fractions as seen in Figure 2(a). Therefore, we conclude that the spread of the neutral fractions is dependent on the initial positioning of each neutral fraction as well as the structure of the mutation matrix.

In addition, we numerically examined a mutation matrix structure that does not satisfy Assumption $A1$ of our main theorems. In particular, we constructed a mutation matrix that is not block diagonal primitive. This matrix is similar to our second example with two mutation classes, but we include a small parameter to introduce a weak linkage between the two mutation classes. This matrix is given by

(26). We see that the weak linkage only allows for individuals to mutate from the second mutation class $\{3, 4, 5\}$ to the first mutation class $\{1, 2\}$. In particular, we see that the weak linkage is a small mutation probability from neutral fraction 3 to 2. Thus, because of this structure, we expect that eventually all individuals will be in the first mutation class regardless of the initial distribution of individuals. The simulation for this example is given in Figure 4. The initial condition for the neutral fractions is seen in Figure 4(a). Then, the dynamics of the neutral fractions is seen in Figures 4(b)-4(d). We see that the asymptotic distribution of neutral fractions is given by the right eigenvector corresponding to eigenvalue 1. However, convergence to the asymptotic distribution takes a long time because of the weak linkage. We conjecture that if the linkage were larger or if there were more linkages then we expect the convergence to the asymptotic proportion would be faster.

We also make the assumption that our growth function is bounded by its value at zero. This assumption does not allow for growth functions with Allee effects which we know from the scalar model to produce interesting asymptotic dynamics (Marculis et al., 2017). By adding the complexity of mutations into the modeling framework, we are able to obtain dynamics that are not seen in scalar models that have no mutations. Unlike the scalar model case, we find that multiple neutral fractions can contribute to the spread of the population in absence of an Allee effect. Thus, we can conclude that these neutral mutations and their structure are an important driver of maintaining genetic diversity in an expanding population. This conclusion agrees with previous studies that have shown range expansions affect the neutral genetic variation of the population (Excoffier et al., 2009; Lehe et al., 2012).

In addition we assume that the dispersal kernel is Gaussian. While this is needed for mathematical convenience, we conjecture that this assumption should be able to be weakened to an assumption that the dispersal kernel is thin-tailed since the results for the asymptotic proportion of each neutral fraction is independent of the parameters from the dispersal kernel. To test this conjecture, we provided simulations for a Laplace dispersal kernel as seen in Figure 3. These simulations show that by only changing the form of the dispersal kernel, we can obtain the same asymptotic proportion of neutral fractions as seen in Figure 2. We were not able to rigorously prove this result and instead leave this conjecture for future analysis.

Other spatial models have shown that neutral mutations at the leading edge of a range expansion sometimes surf on the wave (Edmonds et al., 2004; Klopfstein et al., 2006). In particular, one study found that due to the gene surfing, the mutations reach a larger spatial distribution and higher frequency than would be expected in stationary populations (Edmonds et al., 2004). Our results agree with these studies that the neutral mutations at the leading edge are the drivers of the population spread. However, our model predicts that the spatial distribution of neutral fractions at the leading edge is the same as what would be expected in a stationary population. The primary conclusion for another simulation based model found that the final spatial and frequency distributions depend on the local size of a subdivided population (Klopfstein et al., 2006). We showed that the asymptotic distribution of neutral fractions is dependent on what individuals were at the leading edge, however, our asymptotic proportion we calculate does not depend on on the initial size of the population. We believe that these differences arise because the way we incorporate mutations is deterministic, but gene surfing is an

inherently stochastic process. Thus, in some sense our model describes the average behavior as seen from many realizations of the stochastic process of spread.

Overall, our results show how adding neutral mutations to a model can strongly influence the spread of neutral fractions. We find that the mutation matrix structure and the initial distribution of neutral fractions are important drivers in determining the spread of neutral fractions. However, it should be noted that our model structure is restricted to consider mutations between neutral fractions, so there is no selection occurring in the population dynamics. The mutations are incorporated into the model through a matrix where there are constant probabilities of mutations occurs between individuals. Even though this mutation matrix structure is very general, there are still other ways of including mutation dynamics that could be explored such as including stochastic mutation probabilities. The results we were able to prove in our four theorems relied upon somewhat restrictive assumptions. First, we make the assumption throughout every theorem that the dispersal kernel is Gaussian. However, since our numerical simulations find that our asymptotic proportion does not directly depend on the Gaussian kernel parameters, we conjecture that our result should extend to a larger class of thin-tailed dispersal kernels. Second, the assumption of block diagonal primitivity placed on the mutation matrix is not always satisfied for biological realistic models. We illustrate this with the weak connectivity example.

Appendix A Derivation of a general mutation matrix

Here we show how one can generalize the assumption of a single locus with n different neutral alleles to m loci with two neutral alleles. Let there be m independent loci a_i, $1 \leq i \leq m$, where each loci has one of two possible alleles, $a_i = 0$ or $a_i = 1$. Then we define the transition probabilities as follows:

$$\Pr\{a_i = 0 \to a_i = 1\} = q_i \text{ and } \Pr\{a_i = 1 \to a_i = 0\} = r_i. \tag{27}$$

We index this process by $t \in \mathbb{N}$ where t describes the number of possible transitions taken so far. There are 2^m possible states for this system. Let $n = 2^m$ and let the probability of being in state j, $1 \leq j \leq n$, be given by v^j where the state is

$$j = 1 + \sum_{i=1}^{m} a_i 2^{i-1}. \tag{28}$$

In the case when $m = 2$, there are four total states. We denote our states in the following form,

$$\begin{pmatrix} a_1 \\ a_2 \end{pmatrix}. \tag{29}$$

Our indexing for j gives the following relationship between the state and the index as follows:

Index	$j=1$	$j=2$	$j=3$	$j=4$
State	$\begin{pmatrix}0\\0\end{pmatrix}$	$\begin{pmatrix}1\\0\end{pmatrix}$	$\begin{pmatrix}0\\1\end{pmatrix}$	$\begin{pmatrix}1\\1\end{pmatrix}$

By letting $m_{jl} = \Pr\{v^j \to v^l\}$, then the mutation matrix becomes

$$\mathbf{M} = \begin{bmatrix} (1-q_1)(1-q_2) & r_1(1-q_2) & (1-q_1)r_2 & r_1r_2 \\ q_1(1-q_2) & (1-r_1)(1-q_2) & q_1r_2 & (1-r_1)r_2 \\ (1-q_1)q_2 & r_1q_2 & (1-q_1)(1-r_2) & r_1(1-r_2) \\ q_1q_2 & (1-r_1)q_2 & q_1(1-r_2) & (1-r_1)(1-r_2) \end{bmatrix}. \quad (30)$$

From this example, one can deduce how to generalize this process for more than two neutral alleles making the structure of this mutation matrix quite general.

Appendix B Proofs of the theorems

Proof of Theorem 1

Proof Without loss of generality, we can assume that neutral fraction i belongs to the mutation class q. Then, since $\mathbf{M}$ is block diagonal, we only need to consider the following equation

$$\mathbf{v}_{q,t+1}(x) = \mathbf{M}_q \int_{-\infty}^{\infty} k(x-y) g(u_t(y)) \mathbf{v}_{q,t}(y)\, dy. \quad (31)$$

Using the fact that $0 < g(u) \leq g(0)$ for all $u \in (0,1)$ we can use a comparison principle, see Lemma 2.1 of Li et al. (2005), to show that a new sequence $\mathbf{w}_{q,t}(x)$ defined by

$$\mathbf{w}_{q,t+1}(x) = g(0)\mathbf{M}_q \int_{-\infty}^{\infty} k(x-y) \mathbf{w}_{q,t}(y)\, dy \quad (32)$$

is always greater than the solution to any neutral fraction, $\mathbf{v}_{q,t}(x)$, with the same initial condition $\mathbf{w}_{q,0}(x) = \mathbf{v}_{q,0}(x)$. The solution of (32) is given by the t-fold convolution

$$\mathbf{w}_{q,t}(x) = [g(0)\mathbf{M}_q]^t \, k^{*t} \mathbf{w}_{q,0}(x). \quad (33)$$

Applying the reflected bilateral Laplace transform to (33) and using the convolution theorem, we obtain

$$\begin{aligned} \mathcal{M}[\mathbf{w}_{q,t}(x)](s) &= [g(0)\mathbf{M}_q]^t \left[\mathcal{M}\left[k(x)\right](s)\right]^t \mathcal{M}\left[\mathbf{w}_{q,0}(x)\right](s) && (34) \\ &= [g(0)\mathbf{M}_q]^t \left[e^{\frac{\sigma^2 s^2}{2} + \mu s}\right]^t \mathcal{M}\left[\mathbf{w}_{q,0}(x)\right](s) && (35) \\ &= [g(0)\mathbf{M}_q]^t e^{\frac{\sigma^2 t s^2}{2} + \mu t s} \mathcal{M}\left[\mathbf{w}_{q,0}(x)\right](s) && (36) \\ &= [g(0)\mathbf{M}_q]^t \mathcal{M}\left[\frac{1}{\sqrt{2\pi\sigma^2 t}} e^{-\frac{(x-\mu t)^2}{2\sigma^2 t}}\right](s) \mathcal{M}\left[\mathbf{w}_{q,0}(x)\right](s) && (37) \\ &= [g(0)\mathbf{M}_q]^t \mathcal{M}\left[(k_t * \mathbf{w}_{q,0})(x)\right](s) && (38) \end{aligned}$$

where k_t is Gaussian with mean μt and variance $\sigma^2 t$. Then applying the inverse transform yields

$$\begin{aligned} \mathbf{w}_{q,t}(x) &= [g(0)\mathbf{M}_q]^t (k_t * \mathbf{w}_{q,0})(x) && (39) \\ &= [g(0)\mathbf{M}_q]^t \int_{-\infty}^{\infty} \frac{1}{\sqrt{2\pi\sigma^2 t}} e^{-\frac{(x-y-\mu t)^2}{2\sigma^2 t}} \mathbf{w}_{q,0}(y)\, dy. && (40) \end{aligned}$$

In the moving half-frame with fixed $A \in \mathbb{R}$, consider the element $x_0 + ct$ with $c \geq c^* = \sqrt{2\sigma^2 \ln(g(0))} + \mu$. When we rewrite $\mathbf{w}_{q,t}(x)$ in this moving half-frame we have

$$\mathbf{w}_{q,t}(x_0 + ct) = [g(0)\mathbf{M}_q]^t \int_{-\infty}^{\infty} \frac{1}{\sqrt{2\pi\sigma^2 t}} e^{-\frac{(x_0+ct-y-\mu t)^2}{2\sigma^2 t}} \mathbf{w}_{q,0}(y)\, dy. \tag{41}$$

Expanding in the exponential, yields

$$\frac{(x_0 + ct - y - \mu t)^2}{2\sigma^2 t} = \frac{(x_0 - y)^2}{2\sigma^2 t} + \frac{2(c-\mu)t(x_0 - y) + (c-\mu)^2 t^2}{2\sigma^2 t} \tag{42}$$

$$\geq \frac{(x_0 - y)^2}{2\sigma^2 t} + \frac{c-\mu}{\sigma^2}(x_0 - y) + \ln(g(0))t. \tag{43}$$

Thus,

$$\mathbf{w}_{q,t}(x_0 + ct) \leq \mathbf{M}_q^t \frac{e^{\ln(g(0))t}}{\sqrt{2\pi\sigma^2 t}} \int_{-\infty}^{\infty} e^{-\frac{(x_0-y)^2}{2\sigma^2 t}} e^{-\frac{c-\mu}{\sigma^2}(x_0-y)} e^{-\ln(g(0))t} \mathbf{w}_{q,0}(y)\, dy \tag{44}$$

$$= \mathbf{M}_q^t \frac{1}{\sqrt{2\pi\sigma^2 t}} \int_{-\infty}^{\infty} e^{-\frac{(x_0-y)^2}{2\sigma^2 t}} e^{-\frac{c-\mu}{\sigma^2}(x_0-y)} \mathbf{w}_{q,0}(y)\, dy \tag{45}$$

$$= \mathbf{M}_q^t \frac{e^{-\frac{c-\mu}{\sigma^2}x_0}}{\sqrt{2\pi\sigma^2 t}} \int_{-\infty}^{\infty} e^{-\frac{(x_0-y)^2}{2\sigma^2 t}} e^{\frac{c-\mu}{\sigma^2}y} \mathbf{w}_{q,0}(y)\, dy. \tag{46}$$

Since $x_0 \geq A$ we have

$$\mathbf{w}_{q,t}(x_0 + ct) \leq \mathbf{M}_q^t \frac{e^{-\frac{A(c-\mu)}{\sigma^2}}}{\sqrt{2\pi\sigma^2 t}} \int_{-\infty}^{\infty} e^{\frac{c-\mu}{\sigma^2}y} \mathbf{w}_{q,0}(y)\, dy. \tag{47}$$

Since $\mathbf{M}_q$ is a Markov matrix, we know that $\lim_{t\to\infty} \mathbf{M}_q^t = [\mathbf{r}_q, \ldots, \mathbf{r}_q]$ where $\mathbf{r}_q$ is the right eigenvector of $\mathbf{M}_q$ corresponding to eigenvalue 1 such that $\sum_{i=1} r_{q,i} = 1$. By Assumption *A*4, $\int_{-\infty}^{\infty} e^{\frac{c-\mu}{\sigma^2}y} w_{q,0}^i(y)\, dy < \infty$ for every i in mutation class q we have $w_{q,t}^i(x_0 + ct) \to 0$ uniformly as $t \to \infty$ in $[A, \infty)$. Recall that w_q^i was constructed so that $0 \leq v_{q,t}^i(x) \leq w_{q,t}^i(x)$. This implies the uniform convergence of $v_t^i(x) \to 0$ as $t \to \infty$ in the moving half-frame $[A + ct, \infty)$ for each i in mutation class q. The proof of Theorem 1 is complete. □

Proof of Theorem 2

Proof Repeat the proof of Theorem 1 in the left moving half-frame with fixed $A \in \mathbb{R}$ and consider the element $x_0 - ct$ with $c \geq c_-^* = \sqrt{2\sigma^2 \ln(g(0))} - \mu$. From this change, the result follows in the same manner as in Theorem 1. □

Proof of Theorem 3

Proof We begin by decomposing $\mathbb{R}^n$ according to the eigenspace of the matrix $\mathbf{M}_q$. By assumption, since all the blocks in $\mathbf{M}$ are primitive, we know that the principle eigenvalue is simple and equal to 1 with nonnegative eigenvector $\mathbf{r}_q$ because $\mathbf{M}_q$ is Markov. With a small abuse of notation, we call $\mathbf{r}_q$ the eigenvector of $\mathbf{M}$ associated to the eigenvalue 1 coming from the matrix $\mathbf{M}_q$. In a similar manner, we define

$\boldsymbol{\ell}_q$ be the eigenvector of $\mathbf{M}^T$ associated to the eigenvalue 1 from the matrix $\mathbf{M}_q^T$. Moreover, since the mutation matrix $\mathbf{M}$ is block diagonal, we can decompose the space $\mathbb{R}^n$ as follows

$$\mathbb{R}^n = \bigoplus_{q=1}^{n_q} \mathbf{r}_q\mathbb{R} \bigoplus_{q=1}^{n_q} (\mathbf{r}_q\mathbb{R})^{\perp} \tag{48}$$

where $(\mathbf{r}_q\mathbb{R})^{\perp} = \left\{\mathbf{v} \in \mathbb{R}^n, \mathbf{v}^T\boldsymbol{\ell}_q = \mathbf{0}\right\}$. Let $\mathbf{v}_0(x)$ satisfy $0 \leq v_0^i(x) \leq u_0(x)$ in $\mathbb{R}$ for $i = 1, \ldots, n$. Then, we can decompose $\mathbf{v}_t(x)$ as follows

$$\mathbf{v}_t(x) = \sum_{q=1}^{n_q} a_t^q(x)\mathbf{r}_q + \sum_{q=1}^{n_q} b_t^q(x)\mathbf{h}_t^q \tag{49}$$

where $a_t^q(x)$ and $b_t^q(x)$ are functions from $\mathbb{R}$ to $\mathbb{R}$ and $\mathbf{h}_t^q$ are in $(\mathbf{r}_q\mathbb{R})^{\perp}$ with $\|\mathbf{h}_t^q\| = 1$. Then by applying our decomposition to (3) we can see that

$$\mathbf{v}_{t+1}(x) = \int_{-\infty}^{\infty} k(x-y)g(u_t(y))\mathbf{M}\mathbf{v}_t(y)\,dy \tag{50}$$

$$= \int_{-\infty}^{\infty} k(x-y)g(u_t(y))\mathbf{M}\left(\sum_{q=1}^{n_q} a_t^q(y)\mathbf{r}_q + \sum_{q=1}^{n_q} b_t^q(y)\mathbf{h}_t^q\right)\,dy \tag{51}$$

$$= \sum_{q=1}^{n_q}\int_{-\infty}^{\infty} k(x-y)g(u_t(y))a_t^q(y)\,dy\mathbf{M}\mathbf{r}_q + \sum_{q=1}^{n_q}\int_{-\infty}^{\infty} k(x-y)g(u_t(y))b_t^q(y)\,dy\mathbf{M}\mathbf{h}_t^q. \tag{52}$$

Since $\mathbf{M}\mathbf{r}_q = \mathbf{r}_q$ and $\mathbf{M}$ stabilizes the space $(\mathbf{r}_q\mathbb{R})^{\perp}$, we can see from (49) and (52) that for all $q \in \{1, \ldots, n_q\}$ and $t > 0$

$$a_{t+1}^q(x) = \int_{-\infty}^{\infty} k(x-y)g(u_t(y))a_t^q(y)\,dy \text{ and} \tag{53}$$

$$b_{t+1}^q(x)\mathbf{h}_{t+1}^q = \int_{-\infty}^{\infty} k(x-y)g(u_t(y))b_t^q(y)\,dy\mathbf{M}\mathbf{h}_t^q. \tag{54}$$

We first focus our attention on (54). By the properties of $\mathbf{M}$ through the matrices $\mathbf{M}_q$ there exists $\delta \in (0,1)$ such that for any $q \in \{1, \ldots, n_q\}$ and $\mathbf{h} \in (\mathbf{r}_q\mathbb{R})^{\perp}$ then $\|\mathbf{M}\mathbf{h}\| \leq \delta\|\mathbf{h}\|$. Thus, from (54) we can see that

$$|b_{t+1}^q(x)| = \|b_{t+1}^q(x)\mathbf{h}_{t+1}^q\| \tag{55}$$

$$\leq \int_{-\infty}^{\infty} k(x-y)g(u_t(y))|b_t^q(y)|\,dy\|\mathbf{M}\mathbf{h}_t^q\| \tag{56}$$

$$\leq \delta\int_{-\infty}^{\infty} k(x-y)g(u_t(y))u_t(y)\frac{|b_t^q(y)|}{u_t(y)}\,dy. \tag{57}$$

Since $0 \leq v_0^i(x) \leq u_0(x)$ for all $x \in \mathbb{R}$ for $i = 1, \ldots, n$, it is clear that $|b_0^q(x)| \leq \delta' u_0(x)$ for all $x \in \mathbb{R}$ where $0 < \delta' \leq 1$. From iteration of (57) we have that

$$|b_{t+1}^q(x)| \leq \delta^t\delta' \max_{x\in\mathbb{R}} \|u_0(x)\|. \tag{58}$$

Since $\delta \in (0,1)$,

$$\lim_{t\to\infty} |b_{t+1}^q(x)| \leq \lim_{t\to\infty} \delta^t \delta' \max_{x\in\mathbb{R}} \|u_0(x)\| \tag{59}$$

$$= 0. \tag{60}$$

Thus, $b_{t+1}^q(x)$ converges uniformly to 0 on $\mathbb{R}$. Next, we turn our attention to the remaining piece of our decomposition for $a_t^q(x)$. First, it is important to note that $a_0^q(x)$ is a projection of $\mathbf{v}_0(x)$ on $\mathbf{r}_q$. Thus, it satisfies

$$a_0^q(x) = \frac{\mathbf{v}_0(x)^T \boldsymbol{\ell}_q}{\mathbf{r}_q^T \boldsymbol{\ell}_q}. \tag{61}$$

From our assumption that the mutation class q is present at the leading edge of the front we have

$$\frac{a_0^q(x)}{u_0(x)} \to p_0^q > 0 \text{ as } x \to \infty \text{ and } \int_{-\infty}^{\infty} e^{\frac{c-\mu}{\sigma^2} y} \left| a_0^q(y) - p_0^q u_0(y) \right| \, dy < \infty. \tag{62}$$

Next, we consider the sequence $|z_t(x)| = |a_t^q(x) - p_0^q u_t(x)|$ that satisfies

$$|z_{t+1}(x)| \leq \int_{-\infty}^{\infty} k(x-y) g(u_t(y)) |z_t(y)| \, dy \tag{63}$$

with $|z_0(x)| = |a_0^q(x) - p_0^q u_0(x)|$. By the assumption that $0 < g(u) \leq g(0)$ for all $u \in (0,1)$ we obtain a super-solution

$$|z_{t+1}(x)| \leq g(0) \int_{-\infty}^{\infty} k(x-y) |z_t(y)| \, dy \tag{64}$$

with same initial condition. The solution of (64) is bounded by the t-fold convolution

$$|z_t(x)| \leq [g(0)]^t \, k^{*t} |z_0(x)|. \tag{65}$$

Applying the reflected bilateral Laplace transform to (65) and using the convolution theorem, we obtain

$$\mathcal{M}[|z_t(x)|](s) \leq [g(0)]^t \left[\mathcal{M}\left[k(x)\right](s)\right]^t \mathcal{M}\left|z_0(x)|\right](s) \tag{66}$$

$$= [g(0)]^t \left[e^{\frac{\sigma^2 s^2}{2} + \mu s} \right]^t \mathcal{M}\left[|z_0(x)|\right](s) \tag{67}$$

$$= [g(0)]^t e^{\frac{\sigma^2 t s^2}{2} + \mu t s} \mathcal{M}\left[|z_0(x)|\right](s) \tag{68}$$

$$= [g(0)]^t \mathcal{M}\left[\frac{1}{\sqrt{2\pi\sigma^2 t}} e^{-\frac{(x-\mu t)^2}{2\sigma^2 t}} \right](s) \mathcal{M}\left[|z_0(x)|\right](s) \tag{69}$$

$$= [g(0)]^t \mathcal{M}\left[(k_t * |z_0|)(x)\right](s) \tag{70}$$

where k_t is Gaussian with mean μt and variance $\sigma^2 t$. Then applying the inverse transform yields

$$|z_t(x)| \leq [g(0)]^t (k_t * |z_0|)(x) \tag{71}$$

$$= [g(0)]^t \int_{-\infty}^{\infty} \frac{1}{\sqrt{2\pi\sigma^2 t}} e^{-\frac{(x-y-\mu t)^2}{2\sigma^2 t}} |z_0(y)| \, dy. \tag{72}$$

In the moving half-frame with fixed $A \in \mathbb{R}$, consider the element $x_0 + ct$ with $c \geq c^* = \sqrt{2\sigma^2 \ln(g(0))} + \mu$. When we rewrite $|z_t(x)|$ in this moving half-frame we have

$$|z_t(x_0 + ct)| \leq [g(0)]^t \int_{-\infty}^{\infty} \frac{1}{\sqrt{2\pi\sigma^2 t}} e^{-\frac{(x_0+ct-y-\mu t)^2}{2\sigma^2 t}} |z_0(y)|\, dy. \tag{73}$$

Expanding in the exponential, yields

$$\frac{(x_0 + ct - y - \mu t)^2}{2\sigma^2 t} = \frac{(x_0 - y)^2}{2\sigma^2 t} + \frac{2(c-\mu)t(x_0 - y) + (c-\mu)^2 t^2}{2\sigma^2 t} \tag{74}$$

$$\geq \frac{(x_0 - y)^2}{2\sigma^2 t} + \frac{c-\mu}{\sigma^2}(x_0 - y) + \ln(g(0))t. \tag{75}$$

Thus,

$$|z_t(x_0 + ct)| \leq \frac{e^{\ln(g(0))t}}{\sqrt{2\pi\sigma^2 t}} \int_{-\infty}^{\infty} e^{-\frac{(x_0-y)^2}{2\sigma^2 t}} e^{-\frac{c-\mu}{\sigma^2}(x_0-y)} e^{-\ln(g(0))t} |z_0(y)|\, dy \tag{76}$$

$$= \frac{1}{\sqrt{2\pi\sigma^2 t}} \int_{-\infty}^{\infty} e^{-\frac{(x_0-y)^2}{2\sigma^2 t}} e^{-\frac{c-\mu}{\sigma^2}(x_0-y)} |z_0(y)|\, dy \tag{77}$$

$$= \frac{e^{-\frac{c-\mu}{\sigma^2}x_0}}{\sqrt{2\pi\sigma^2 t}} \int_{-\infty}^{\infty} e^{-\frac{(x_0-y)^2}{2\sigma^2 t}} e^{\frac{c-\mu}{\sigma^2}y} |z_0(y)|\, dy. \tag{78}$$

Since $x_0 \geq A$ we have

$$|z_t(x_0 + ct)| \leq \frac{e^{-\frac{A(c-\mu)}{\sigma^2}}}{\sqrt{2\pi\sigma^2 t}} \int_{-\infty}^{\infty} e^{\frac{c-\mu}{\sigma^2}y} |z_0(y)|\, dy. \tag{79}$$

From our assumption that the mutation class q is initially present at the leading edge of the front, we know that $\int_{-\infty}^{\infty} e^{\frac{c-\mu}{\sigma^2}y} |z_0(y)|\, dy < \infty$ Thus, we have that $|z_t(x)| \to 0$ uniformly as $t \to \infty$ in the moving half-frame $[A + ct, \infty)$ with speed $c \geq c^*$. Returning to the definition of $|z_t(x)|$ we can see that

$$|a_t^q(x) - p_0^q u_t(x)| \to 0 \text{ uniformly as } t \to \infty \tag{80}$$

in the moving half-frame $[A + ct, \infty)$. Then by putting together all the pieces, we can see from (49) that

$$\left\| \mathbf{v}_t(x) - \sum_{q=1}^{n_q} a_t^q(x) \mathbf{r}_q \right\| = \left\| \sum_{q=1}^{n_q} b_t^q(x) \mathbf{h}_t^q \right\| \tag{81}$$

$$\leq \sum_{q=1}^{n_q} |b_t^q(x)| \|\mathbf{h}_t^q\| \tag{82}$$

$$= \sum_{q=1}^{n_q} |b_t^q(x)| \tag{83}$$

Therefore, from (60) and (80) the we can conclude that

$$\max_{[A+ct,\infty)} \left\| \mathbf{v}_t(x) - \sum_{q=1}^{n_q} p_0^q u_t(x) \mathbf{r}_q \right\| \to 0 \text{ as } t \to \infty. \tag{84}$$

The proof of Theorem 3 is complete. □

Proof of Theorem 4

Proof Repeat the proof of Theorem 3 in the left moving half-frame with fixed $A \in \mathbb{R}$ and consider the element $x_0 - ct$ with $c \geq c_-^* = \sqrt{2\sigma^2 \ln(g(0))} - \mu$. From this change, the result follows in the same manner as in Theorem 3. □

References

Arenas M. Trends in substitution models of molecular evolution. Front Genet, 6: 319, 2015.

Bateman AW, Buttenschön A, Erickson KD, and Marculis NG. Barnacles vs bullies: modelling biocontrol of the invasive european green crab using a castrating barnacle parasite. Theor Ecol, 10(3):305–318, 2017.

Bonnefon O, Garnier J, Hamel F, and Roques L. Inside dynamics of delayed travelling waves. Math Mod Nat Phen, 8:44–61, 2013.

Bonnefon O, Coville J, Garnier J, and Roques L. Inside dynamics of solutions of integro-differential equations. Discret Contin Dyn Syst - Ser B, 19(10):3057–3085, 2014.

Bromham L and Penny D. The modern molecular clock. Nat Rev Genet, 4(3): 216, 2003.

Cooley JW and Tukey JW. An algorithm for the machine calculation of complex fourier series. Math Comput, 19(90):297–301, 1965.

Duret L. Neutral theory: the null hypothesis of molecular evolution. Nature Education, 1:803–806, 2008.

Edmonds CA, Lillie AS, and Cavalli-Sforza LL. Mutations arising in the wave front of an expanding population. Proc Natl Acad Sci, 101(4):975–979, 2004.

Excoffier L and Ray N. Surfing during population expansions promotes genetic revolutions and structuration. Trends Ecol Evol, 23(7):347–351, 2008.

Excoffier L, Foll M, and Petit RJ. Genetic consequences of range expansions. Annu Rev of Ecol Evol Syst, 40:481–501, 2009.

Felsenstein J. Evolutionary trees from dna sequences: a maximum likelihood approach. J Mol Evol, 17(6):368–376, 1981.

Garnier J and Lewis MA. Expansion under climate change: the genetic consequences. Bull Math Biol, 78(11):2165–2185, 2016.

Garnier J, Giletti T, Hamel F, and Roques L. Inside dynamics of pulled and pushed fronts. J des Math Pures Appl, 98(4):428–449, 2012.

Hallatschek O and Nelson DR. Gene surfing in expanding populations. Theor Popul Biol, 73(1):158–170, 2008.

Hallatschek O, Hersen P, Ramanathan S, and Nelson DR. Genetic drift at expanding frontiers promotes gene segregation. Proc Natl Acad Sci, 104(50): 19926–19930, 2007.

Ho S. The molecular clock and estimating species divergence. Nature Education, 1(1):1–2, 2008.

Jukes T and Cantor C. Evolution of protein molecules. in 'mammalian protein metabolism'.(ed. hn munro.) pp. 21–132, 1969.

Kimura M. A simple method for estimating evolutionary rates of base substitutions through comparative studies of nucleotide sequences. J Mol Evol, 16(2):111–120, 1980.

Klopfstein S, Currat M, and Excoffier L. The fate of mutations surfing on the wave of a range expansion. Mol Biol Evol, 23(3):482–490, 2006.

Kot M, Lewis MA, and van den Driessche P. Dispersal data and the spread of invading organisms. Ecology, 77(7):2027–2042, 1996.

Krkošek M, Lauzon-Guay JS, and Lewis MA. Relating dispersal and range expansion of california sea otters. Theor Popul Biol, 71(4):401–407, 2007.

Lande R. Neutral theory of quantitative genetic variance in an island model with local extinction and colonization. Evolution, 46(2):381–389, 1992.

Lehe R, Hallatschek O, and Peliti L. The rate of beneficial mutations surfing on the wave of a range expansion. PLoS Comput Biol, 8(3):e1002447, 2012.

Lewis MA, Petrovskii SV, and Potts JR. The Mathematics Behind Biological Invasions, volume 44. Springer, 2016.

Lewis MA, Marculis NG, and Shen Z. Integrodifference equations in the presence of climate change: persistence criterion, travelling waves and inside dynamics. J Math Biol, 77(6-7):1649–1687, 2018.

Li B, Weinberger HF, and Lewis MA. Spreading speeds as slowest wave speeds for cooperative systems. Math Biosci, 196(1):82–98, 2005.

Lui R. Existence and stability of travelling wave solutions of a nonlinear integral operator. J Math Biol, 16(3):199–220, 1983.

Lutscher F, Pachepsky E, and Lewis MA. The effect of dispersal patterns on stream populations. SIAM Rev, 47(4):749–772, 2005.

Lynch M. The divergence of neutral quantitative characters among partially isolated populations. Evolution, 42(3):455–466, 1988.

Marculis NG, Lui R, and Lewis MA. Neutral genetic patterns for expanding populations with nonoverlapping generations. Bull Math Biol, 79(4):828–852, 2017.

Marculis NG, Garnier J, Lui R, and Lewis MA. Inside dynamics for stage-structured integrodifference equations. J Math Biol, In Press, 2019.

Mayr E. Speciation phenomena in birds. Am Nat, 74(752):249–278, 1940.

Morin PA, Luikart G, and Wayne RK. Snps in ecology, evolution and conservation. Trends Ecol Evol, 19(4):208–216, 2004.

Pannell JR and Charlesworth B. Neutral genetic diversity in a metapopulation with recurrent local extinction and recolonization. Evolution, 53(3):664–676, 1999.

Pannell JR and Charlesworth B. Effects of metapopulation processes on measures of genetic diversity. Philosophical Transactions of the Royal Society of London. Series B: Biological Sciences, 355(1404):1851–1864, 2000.

Reimer JR, Bonsall MB, and Maini PK. Approximating the critical domain size of integrodifference equations. Bull Math Biol, 78(1):72–109, 2016.

Roques L, Garnier J, Hamel F, and Klein EK. Allee effect promotes diversity in traveling waves of colonization. Proc Natl Acad Sci, 109(23):8828–8833, 2012.

Roques L, Hosono Y, Bonnefon O, and Boivin T. The effect of competition on the neutral intraspecific diversity of invasive species. J Math Biol, 71(2):465–489, 2015.

Selkoe KA and Toonen RJ. Microsatellites for ecologists: a practical guide to using and evaluating microsatellite markers. Ecol Lett, 9(5):615–629, 2006.

Slatkin M. Gene flow in natural populations. Annual review of ecology and systematics, 16(1):393–430, 1985.

Slatkin M and Excoffier L. Serial founder effects during range expansion: a spatial analog of genetic drift. Genetics, 191(1):171–181, 2012.

Stokes A. On two types of moving front in quasilinear diffusion. Math Biosci, 31 (3-4):307–315, 1976.

Van Kirk RW and Lewis MA. Integrodifference models for persistence in fragmented habitats. Bull Math Biol, 59(1):107, 1997.

Weinberger HF. Long-time behavior of a class of biological models. SIAM J Math Anal, 13(3):353–396, 1982.

Zhou Y and Kot M. Discrete-time growth-dispersal models with shifting species ranges. Theor Ecol, 4(1):13–25, 2011.